Full-range debonding analysis between a thin plate and a curved quasi-brittle substrate

Full-range debonding analysis between a thin plate and a curved quasi-brittle substrate

Laura De Lorenzis, Giorgio Zavarise
Department of Innovation Engineering, University of Salento, Italy
laura.delorenzis@unisalento.it, giorgio.zavarise@unisalento.it

Keywords: cohesive zone modeling, curved substrate, fracture mechanics, interface debonding

1. INTRODUCTION AND PROBLEM DEFINITION

The mechanics of interfacial bond between a thin plate and a flat quasi-brittle substrate under mode-II loading has been extensively studied [1]. A typical example is given by fiber-reinforced polymer (FRP) strips bonded to concrete or masonry. Surprisingly, limited attention has been devoted to members with a curved surface, despite the fact that such members are often found in practice [2]. The strengthening of a masonry arch with FRP strips to inhibit the formation of hinges constitutes a typical example. If the FRP strip is placed at the intrados, the interfacial normal (peeling) tensile stresses are likely to lead to mixed-mode fracture of the masonry substrate. Thus they may accelerate debonding with respect to the mode-II fracture case [3]. Debonding phenomena have been observed in several experiments on arches strengthened at the intrados, so that the use of anchoring devices as preventive measures has been proposed [4]. However, neither analytical nor numerical approaches have been proposed so far to tackle the problem from a mechanical standpoint.

This paper deals with modeling of the interface between a rigid substrate with simple curvature and a thin bonded plate. The attention is focused first on the pre-debonding phase. An analytical model is proposed, where the interfacial behavior is modeled by independent bilinear cohesive zone (CZ) laws in the normal and tangential directions, coupled with a mixed-mode fracture criterion. The analytical model permits to determine the interfacial shear and normal stress distributions along the bond length as functions of the substrate curvature, during the various behavioral stages of the interface prior to the initiation of debonding. The evolution of the interface from the initial stage of loading up to the onset of debonding can thus be examined. The model is also capable of predicting the debonding load. Subsequently, the debonding process is analyzed. To this aim, a second analytical model based on linear-elastic fracture mechanics (LEFM) is proposed, which is able to predict the load at onset of debonding and the subsequent behavior of the joint. The two models collectively enable the evaluation of the effects of curvature on the full-range behavior of bonded joints. Finally, a numerical model is devised for comparison and verification of the analytical results.

The models consider a thin plate of thickness t, unit width and length L, made of a linearly elastic material with elastic modulus E. The plate is bonded to a rigid substrate with a constant in-plane curvature radius, r, and loaded with a force F (Figure 1). The force direction is initially tangent to the substrate surface at the loaded (right) end. To map the interface behavior, the curvilinear coordinate, s, is introduced, with origin at the plate free end. Normal and tangential stresses, p_N and p_T, arise at the interface between the plate and the substrate. Both of them are considered uniform across the thickness of the adhesive layer.

2. CZ MODEL: INTERFACIAL STRESSES AND INITIATION OF DEBONDING

Independent bilinear cohesive laws are considered in the normal and tangential directions (Figure 2). Tension relates the normal relative displacement of the bonded surfaces, $g_N > 0$, and

the normal stress, p_N, while shear relates the tangential relative displacement, g_T, and the tangential stress, p_T. The classical linear mixed-mode fracture criterion is introduced to couple the two laws in the instant of debonding, as follows

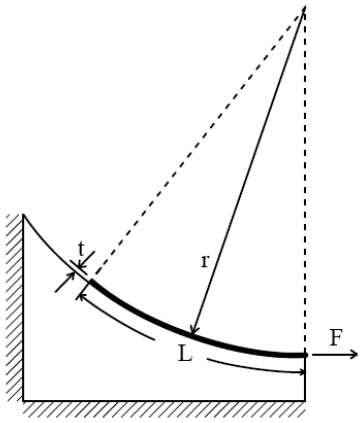

Figure 1. Problem definition.

$$\frac{G_I}{G_{If}} + \frac{G_{II}}{G_{IIf}} = 1 \tag{1}$$

where the energy release rates in mode I and mode II, G_I and G_{II}, are identified as the areas under the respective cohesive laws integrated up to the current values of g_N and g_T. Moreover, G_{If} and G_{IIf} denote, respectively, the fracture energies in pure mode-I and mode-II conditions. These are given by the total areas underneath the respective cohesive zone laws.

The choice of independent cohesive zone laws gives the model a level of simplicity amenable to the obtainment of an analytical solution. It is also motivated by the lack of any experimental basis for the adoption of a given coupled law for the main application under consideration (namely, bond of FRP to concrete or masonry substrates). Finally, this choice enables the use of different values for the mode-I and mode-II interfacial fracture energies, in agreement with the experimental evidence.

The governing equations of the problem are found using the equilibrium of forces for the differential element of the plate, the linearly elastic behavior of the plate material, and the compatibility equations. These are combined with the assumptions of rigid substrate, and of small thickness of the plate. In particular, both the plate bending and shear stiffnesses are neglected, therefore only axial forces are considered. For the detailed development of the model, see [5].

For small loads, the whole length of the interface is at the elastic stage in both the tangential and the normal directions (i.e. the interfacial stresses both fall within the first branch of the respective cohesive laws), and no softening or debonding occur. Representative results for the interfacial stresses are shown in Figure 3 (for details about the parameters, see the section "Results"). Note that the zero shear stress condition at the loaded end is not satisfied, which is typical of first-order solutions [2].

The force $F_{el,T}$, for which the interface would enter the softening stage in the tangential direction, while still being at the elastic stage in the normal direction, is given by [5]

$$F_{el,T} = p_{T\max} \frac{\tanh(\lambda_r L)}{\lambda_r} \tag{2}$$

where

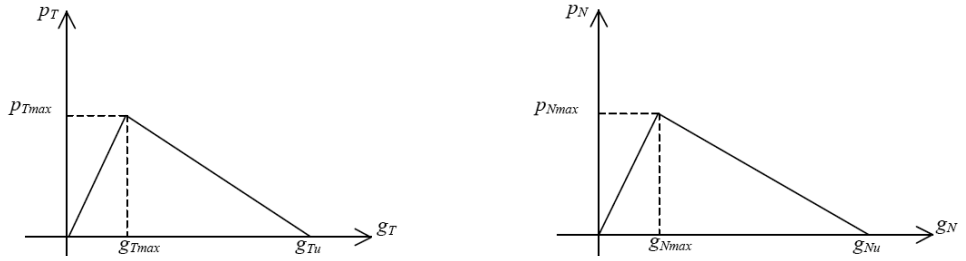

(a) Shear (b) Tension

Figure 2. Interfacial cohesive laws.

$$\lambda_r^2 = \frac{p_{T\max}}{g_{T\max} Et}\left(1 - \frac{g_{N\max} Et}{p_{N\max} r^2}\right) \tag{3}$$

In eq. (3), $p_{N\max}$ and $p_{T\max}$ are the peak values of the normal and shear stresses in the respective cohesive laws, and $g_{N\max}$ and $g_{T\max}$ are the corresponding values of the normal and shear relative displacements (Figure 2). Conversely, the force $F_{el,N}$, for which the interface would enter the softening stage in the normal direction, while still being at the elastic stage in the tangential direction, is [5]

$$F_{el,N} = p_{N\max} r \tag{4}$$

For practical values of the parameters, it is $F_{el,T} < F_{el,N}$, hence the softening stage is entered in the tangential direction first. As loading progresses, an increasingly long portion of the interface closest to loaded end of the plate enters the softening stage in the tangential direction, while the rest remains at the elastic stage. In the normal direction, the interface stays at the elastic stage along the whole length of the joint. Representative curves for the interfacial stresses in these conditions are given in Figure 4. The onset of debonding is reached during this stage, provided that the corresponding load is smaller than $F_{el,N}$. In summary, in this case it is $F_{el,T} < F_{deb} < F_{el,N}$, where F_{deb} is the debonding load. Debonding is triggered by the combination of the interfacial tangential and normal stresses, according to the mixed-mode fracture criterion in eq. (1). Representative load-displacement curves are given in Figure 5.

Other cases, where debonding is triggered by normal stresses and $F_{deb} = F_{el,N}$, are also possible. However, they are unlikely for realistic values of the geometry, material and cohesive zone parameters in the main application under study, i.e. strengthening of a masonry arch with FRP sheets. For a detailed treatment of all the possible cases, see [5].

Once debonding is initiated, the proposed model can no longer follow the behavior of the joint. In fact, assuming that the applied force maintains the initial direction during debonding, the presence of bending and shear forces can no longer be neglected and a new model is needed.

3. LEFM MODEL: INITIATION AND PROGRESSION OF DEBONDING

It is useful to recall here the key results relative to the problem of a thin plate subjected to inclined loading in the peel test configuration with a peel angle β [6]. It is assumed that the applied load maintains its direction during the debonding process, and that the mixed-mode fracture criterion in eq. (1) holds. Under these assumptions, the steady-state peeling load, F_{peel}, takes the following expression

$$\frac{F_{peel}}{G_{If}} = \frac{\sqrt{\left(\frac{Et}{G_{If}}\right)^2 (1-\cos\beta)^2 + 2\frac{Et}{G_{If}}\left(\sin^2\beta + k\cos^2\beta\right) - \frac{Et}{G_{If}}(1-\cos\beta)}}{\left(\sin^2\beta + k\cos^2\beta\right)} \tag{5}$$

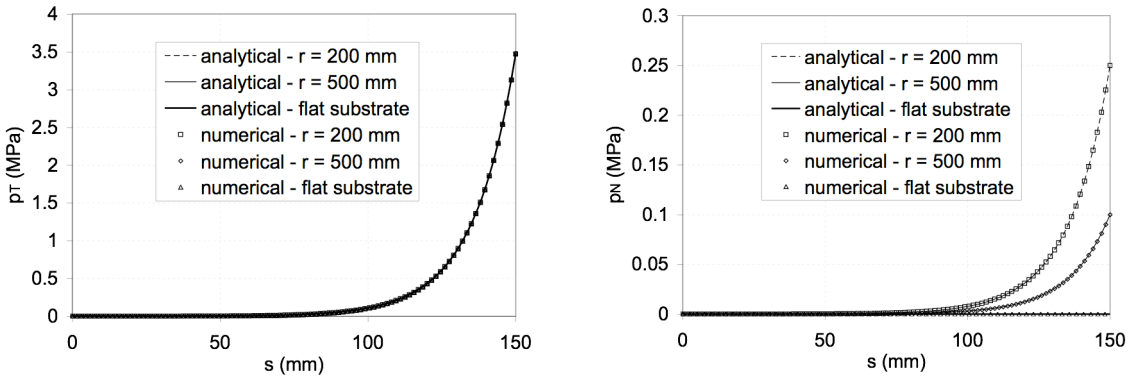

(a) Shear stresses (b) Normal stresses

Figure 3. Interfacial stresses – elastic stage (F = 50 N/mm).

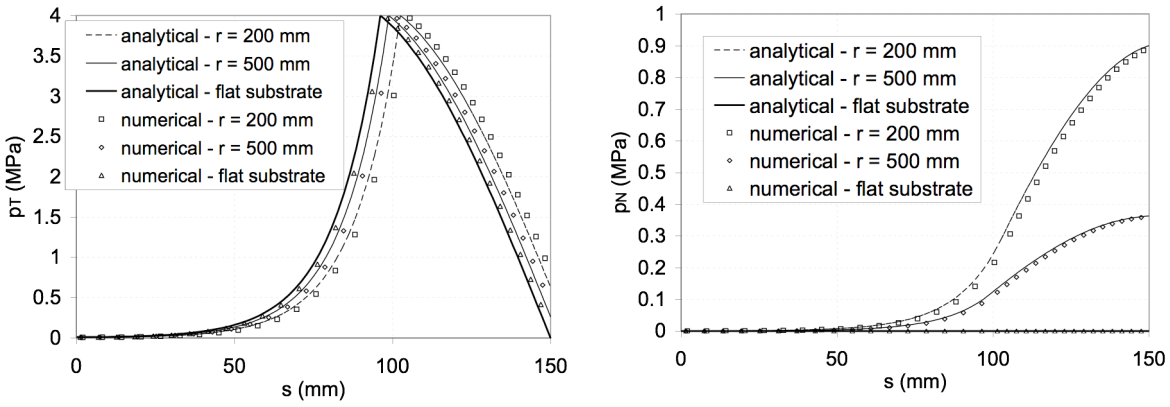

(a) Shear stresses (b) Normal stresses

Figure 4. Interfacial stresses – elastic-softening stage at the initiation of debonding ($F = F_{deb}$).

where $k = G_{If} / G_{IIf}$. This equation shows that the dimensionless steady-state peeling load, F_{peel} / G_{If}, depends on the three dimensionless parameters Et / G_{If}, k and β.

For the current scheme, all the previous equations continue to hold with $\beta = a / r$, where a is the length of an initial debonded portion (crack), and β is the angle formed by the axis of the thin plate with the tangent to the substrate at the crack tip (Figure 6a). Therefore, the initial debonding load, F_{deb}, is given by eq. (5) with $\beta = a / r$.

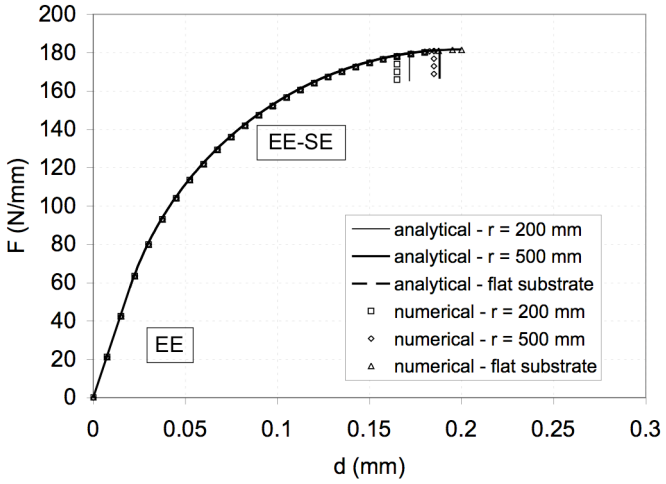

Figure 5. Load vs. loaded-end displacement.

In the particular case of $a = 0$, i.e. for a thin plate starting with the axis tangent to the substrate (Figure 6b), eq. (5) immediately gives

$$F_{deb}(a = 0) = \sqrt{2EtG_{IIf}} \tag{6}$$

that is the well-known expression for the mode-II debonding load of a thin plate bonded to a flat rigid substrate. In other words, according to LEFM predictions, the debonding load of a thin plate is not affected by the curvature of the substrate, but only by the angle between the load and the tangent to the substrate at the loaded end. In particular, it is equal to the pure mode-II debonding load if the plate is tangent to the substrate at the loaded end. This result is an obvious consequence of the fact that LEFM considers a fracture process zone of zero size, located at the crack tip. The crack tip local conditions do not "see" any effect of the substrate curvature but are only influenced by the local peel angle. Conversely, in the CZ model the fracture process zone has a finite size, dictated by the cohesive zone parameters. Hence the curvature effect does influence the debonding load even though the plate is tangent to the substrate at the loaded end. It can be shown [7] that the debonding load predicted by the CZ model reduces to that in eq. (6) when the elastic stiffness and the peak stress of the CZ laws tend to infinity, keeping constant finite fracture energies of the interface.

In the peel test configuration, the angle β formed by the thin plate with the (flat) substrate at the crack tip has a constant value. Conversely, in the current scheme the angle formed by the thin plate with the tangent to the substrate at the crack tip increases as debonding progresses. Therefore, the current scheme can be regarded as a peel test configuration where the peel angle

increases during the progression of debonding. Thus, eq. (5) with $\beta = a / r$ can be used not only to evaluate the debonding load as a function of the initial length of the debonded portion, but also to follow the evolution of the debonding process, if a is intended as the current length of the debonding crack. Figure 7 shows the dimensionless debonding load as a function of the horizontal displacement of the plate loaded end, u (which in turn is a function of a, for details see [7]). It is immediate to observe that, unlike in the case of a flat substrate [1], the debonding process for a curved substrate occurs under a decreasing load, and the rate of the decrease is strongly influenced by the value of the curvature.

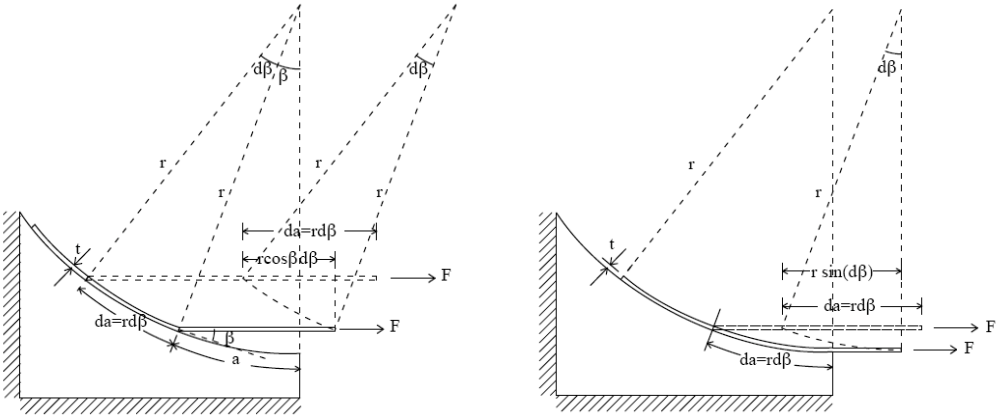

(a) debonding at an angle $\beta = a / r$ (b) debonding at $\beta = 0$

Figure 6. Schematics of the debonding process for a flexible but inestensible thin plate.

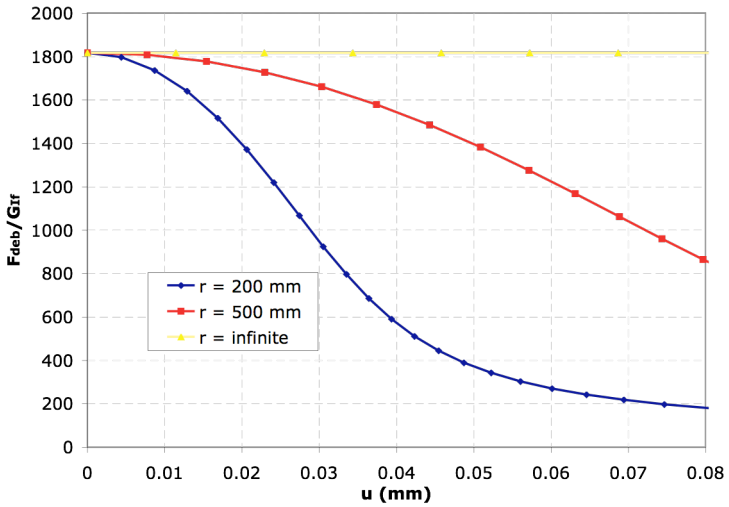

Figure 7. Load vs. loaded-end displacement during debonding.

4. NUMERICAL MODEL

The cohesive models have been implemented into a contact element based on the node-to-segment strategy, as employed in [8], and generalized to handle cohesive forces in both the normal and tangential directions. In the normal direction, under compression the non-penetration condition

is enforced using the penalty method. Depending on the contact status, an automatic switching procedure is used to choose between cohesive and contact models. Each element contribution for the cohesive and contact forces is suitably added to the global virtual work equation.

Figure 8 illustrates two representative finite element meshes. The adherend is modeled with two-dimensional, finite deformation, linearly-elastic beam elements, whereas the substrate is discretized with 4-node isoparametric plane stress elastic elements. The non-linear problem is solved with a Newton-Raphson procedure, where the global tangent stiffness matrix is properly obtained with a consistent linearization of all the contact contributions. The model is implemented in the finite element code FEAP (courtesy of Prof. R.L. Taylor).

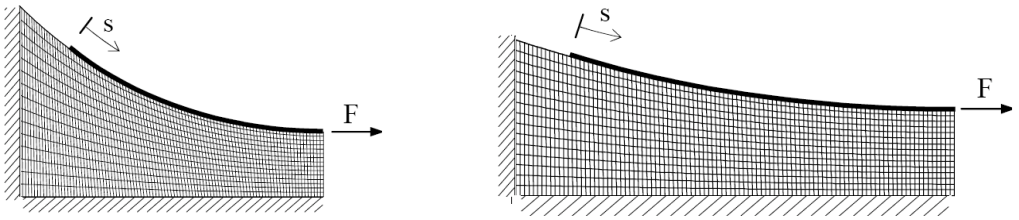

(a) $r = 200$ mm (b) $r = 500$ mm

Figure 8. Mesh used in the numerical analyses.

5. RESULTS

The chosen input values of the example presented are realistic for FRP sheets bonded to a concrete or masonry substrate: $E = 250$ GPa, $t = 0.165$ mm, $p_{N\max} = 2$ MPa, $p_{T\max} = 4$ MPa, $g_{N\max} = 0.01$ mm, $g_{T\max} = 0.02$ mm, $g_{Nu} = 0.1$ mm, $g_{Tu} = 0.2$ mm. The bond length is chosen as $L = 150$ mm. The curvature radii considered are equal 200 mm, 500 mm, and infinite (flat substrate). Figures 3 to 5 and 7 illustrate the results. The values of $F_{el,T}$, $F_{el,N}$ and F_{deb} according to the CZ model are reported in Table 1.

The curves in Figures 3 and 4 clearly show that the substrate curvature has no appreciable effect on the magnitude and distribution of the interfacial shear stresses. Conversely, a significant influence is visible on the interfacial normal stresses. These are identically zero for a flat substrate, and their magnitude increases as the substrate curvature radius decreases. As expected, tensile normal stresses are obtained as a result of the concave shape of the substrate. An excellent agreement is found between analytical and numerical results.

Figure 4 illustrates the interfacial stress distributions at the onset of debonding. In the case of a flat substrate, the interfacial shear stress at debonding reaches zero at the loaded end. This does no longer hold in the case of curved substrates. Debonding is predicted to occur when the boundary of eq. (1) is reached. As the curvature increases this condition is met for a progressively larger value of the interfacial shear stress at the loaded end.

As visible from the values in Table 1, the reduction of the debonding load due to the curvature for the considered example is rather weak. This is due to the fact that the interfacial normal stresses are considerably smaller than the shear stresses, hence the contribution of the mode-I component to the first member of eq. (1) is rather small. In general, the extent to which the debonding load is influenced by the substrate curvature will be a function of the material, geometry and cohesive parameters valid for the interface under examination.

Figure 5 illustrates the load vs. loaded-end displacement curves according to the CZ and numerical models. There is no appreciable influence of the substrate curvature on the obtained behavior, up to the debonding load which is moderately influenced by the curvature as mentioned

earlier. The two stages in the behavior of the interface are clearly visible, with a linear force-displacement relationship during the elastic stage (EE) followed by a non-linear trend during the elastic-softening stage (EE-SE). The analytical and numerical curves are virtually coincident.

As outlined earlier, the load-displacement curves after the initiation of debonding are heavily influenced by the curvature, and their trend as predicted by the LEFM model is shown in Figure 7.

Table 1. $F_{el,T}$, $F_{el,N}$ and F_{deb} for the example (CZ model).

	$F_{el,T}$ (N/mm) (eq. 2)	$F_{el,N}$ (N/mm) (eq. 4)	F_{deb} (N/mm)
r = 200 mm	57.6	400	180.1
r = 500 mm	57.5	1000	181.4
r = ∞	57.4	∞	181.7

6. CONCLUSIONS

Two new analytical models have been developed for the study of debonding between a thin plate and a rigid substrate with simple constant curvature. The CZ analytical model can be used to determine the interfacial shear and normal stresses as functions of the substrate curvature prior to the initiation of debonding, as well as to estimate the debonding load of the joint. The LEFM analytical model is capable of estimating the debonding load, as well as to follow the behavior of the joint during the progression of debonding. Also, a numerical model where the interface is modeled by zero-thickness node-to-segment contact elements has been devised. The numerical model can follow all behavioral stages of the joint, and its results are directly comparable with those of the CZ analytical model. The example shown demonstrates that the presented analytical and numerical models are effective tools to examine the behavior and capacity of a bonded joint in presence of substrate curvature. Further work is needed to investigate numerically the response of the interface if coupled CZ laws are adopted.

References

[1] Yuan, H., Teng, J.G., Seracino, R., Wu, Z.S., Yao, J. "Full-range behaviour of FRP-to-concrete bonded joints". *Engineering Structures*, 26, 2004, 553-565.

[2] De Lorenzis, L., Teng, J.G., Zhang, L. "Elastic interfacial stresses in curved members bonded with a thin plate". *International Journal of Solids and Structures*, 43, 2006, 7501-7517.

[3] CNR-DT 200/2004. "Guide for the Design and Construction of Externally Bonded FRP Systems for Strengthening Existing Structures - Materials, RC and PC structures, masonry structures", CNR, Rome, 2004 (English version).

[4] De Lorenzis, L., Dimitri, R., La Tegola, A. (2007). "Reduction of the lateral thrust of masonry arches and vaults with FRP composites", *Construction and Building Materials*, 21(7), 2007, 1415-1430.

[5] De Lorenzis, L., Zavarise, G. "Interfacial stress analysis and prediction of debonding for a thin plate bonded to a curved substrate", *International Journal of Non-Linear Mechanics*, 2009, in press.

[6] De Lorenzis, L., Zavarise, G. "Modeling of mixed-mode debonding in the peel test applied to superficial reinforcements", *International Journal of Solids and Structures*, 45, 2008, 5419-5436.

[7] De Lorenzis, L., Zavarise, G., "Debonding analysis of thin plates from curved quasi-brittle substrates", journal paper in preparation.

[8] Wriggers, P., Zavarise, G., Zohdi, T.I. "A computational study of interfacial debonding damage in fibrous composite materials". *Computational Materials Science*, 12, 1998, 39-56.